International Journal of Engineering Science 52 (2012) 89–102

Contents lists available at SciVerse ScienceDirect

International Journal of Engineering Science

journal homepage: www.elsevier.com/locate/ijengsci

Compliant substrate controlling the phase diagrams of multiferroic multilayers

Yang-Fan Hu [a,b], Yu-Lan Liu [a,*], Biao Wang [b,*], Yue Zheng [b,*]

[a] Department of Applied Mechanics & Engineering, Sun Yat-Sen University, 510275 Guangzhou, China
[b] State Key Laboratory of Optoelectronic Materials and Technologies, School of Physics and Engineering, Sun Yat-sen University, 510275 Guangzhou, China

ARTICLE INFO

Article history:
Received 29 September 2011
Received in revised form 19 October 2011
Accepted 14 November 2011
Available online 26 December 2011

Keywords:
Multiferroics
Multilayers
Misfit strains
Phase diagrams

ABSTRACT

For a ferroelectric/ferromagnetic multilayer sandwiched between substrates, the tunability of the internal strains, ferroelectric states and phase diagrams by adjusting the substrate thickness are investigated. Based on the continuum mechanics and phenomenological theory, the thermodynamic potentials of the restraint ferroelectric/elastic and ferroelectric/ferromagnetic multilayer are constructed, respectively. Due to the interaction of different layers mediated by the mechanical coupling, the total strains in different layers are solved as functions of the misfit strains, electric polarizations of the ferroelectric slabs and magnetic polarizations of the ferromagnetic slabs. More importantly, the phase diagrams of multiferroic multilayer sandwiched between substrates are comprehensively investigated based on the modified thermodynamic potential. From our results, it can be found that the phase diagrams of the multiferroic multilayers can be effectively shifted by changing the multilayer-substrate thickness ratio, and the phase diagram configuration of the multiferroic multilayer can be dramatically changed by controlling the co-effect of the multilayer-substrate thickness ratio and other tunable quantities, such as multilayer-substrate misfit strains, in-multilayer thickness ratio and in-multilayer misfit strains.

1. Introduction

Last decade has witnessed a revival of research interest on multiferroic materials for interesting science involved and applications of multifunctional devices (Eerenstein, Mathur, & Scott, 2006; Fiebig, 2005; Nan, Bichurin, Dong, Viehland, & Srinivasan, 2008). Magnetoelectric (ME) effect, the most important property of multiferroic materials, refers to the generation of electric polarization **P** when subject to a magnetic field **H** or the generation of magnetic polarization **M** when subject to a electric field **E**. Since multiferroic single crystals are rare (Hill, 2000) and their ME effects are generally very weak or even vanish around room temperature, an alternative choice is to obtain ME effect as a product property from multiferroic composites. These composites are commonly fabricated by bonding ferroelectric materials with strong piezoelectric effect and ferromagnetic materials with strong magnetostrictive effect. Multiferroic multilayers (or called 2-2 type multiferroic composites, Newnham, Skinner, & Cross, 1978) is an essential composite type (Eerenstein, Wiora, Prieto, Scott, & Mathur, 2007; Srinivasan, Rasmussen, & Hayes, 2003; Thiele, Dörr, Bilani, Rödel, & Schultz, 2007; Wang, Zhang, Ma, Lin, & Nan, 2008). High quality multilayer, or its prototype thin film, is obtained by using the technique of epitaxial growth, which provides well mechanical bonding at the interface between film and substrate. Another intrinsic advantage of this technique is that

* Corresponding authors. Tel./fax: +862084115692/3231.
E-mail addresses: stslyl@mail.sysu.edu.cn (Y.-L. Liu), wangbiao@mail.sysu.edu.cn (B. Wang), zhengy35@mail.sysu.edu.cn (Y. Zheng).

0020-7225/$ - see front matter © 2011 Elsevier Ltd. All rights reserved.
doi:10.1016/j.ijengsci.2011.11.008

possible lattice mismatch between the substrate and the thin film causes eigenstrain which strongly affects the physical properties of the upper film layer (Gao & Nix, 1999; Nix, 1989; Saha & Nix, 2002; Suo & Zhang, 1998).

The influence of this strain on ferroelectric and ferromagnetic thin films is widely studied. For ferroelectric thin films, the research topics include tunability of the ferroelectric states of thin film-substrate system by misfit strains (Diéguez et al., 2004; Luo, Wang, & Zheng, 2011; Pertsev, Tagantsev, & Setter, 2000; Pertsev, Kukhar, Kohlstedt, & Waser, 2003; Pertsev, Zembilgotov, & Tagantsev, 1998; Prokhorenko & Pertsev, 2010; Sai, Kolpak, & Rappe, 2005; Sang, Liu, & Fang, 2008; Zembilgotov, Pertsev, Böttger, & Waser, 2005), critical thickness of the ferroelectric thin film and the impact of the misfit strains on its (Junquera & Ghosez, 2003; Wang & Woo, 2005; Zhong, Wang, Zhang, & Qu, 1994), strain relaxation caused by dislocation generation at the interface and its relation to thickness of the thin film (Zheng, Wang, & Woo, 2006a, 2006b; Zheng, Wang, & Woo, 2007), etc. For ferromagnetic thin films, a lot focus has been put on realization of the Giant Magnetoresistance Ratio (GMR) caused by quantum tunnelling effect in ferromagnetic multilayers and superlattices (Bruno & Chappert, 1991; Grünberg, 2000; Ikeda et al., 2007). Although the magnetoelastic coupling in magnetic materials is usually weaker than the electromechanical coupling in ferroelectric materials, regulation of the magnetic polarizations in ferromagnetic thin films through changing the strains is still practical (O'Handley, Murray, Marioni, Nembach, & Allen, 2000; Pertsev, 2008; Thiele et al., 2007).

Multi-scale approaches are used in these researches, including molecular dynamics simulation, first-principle calculation, and phenomenological thermodynamic potential based on Landau-type free energy expansion. Based on the Landau thermodynamic potential, Pertsev et al. (1998) put forward the research on misfit strain-temperature phase diagrams for ferroelectric epitaxial thin films. The phase diagrams for $BaTiO_3$ and $PbTiO_3$ thin films are studied in his work, from which all possible phases as well as tunability of the physical properties by adjusting the misfit strains at the thin film-substrate interface are obtained. Since then, a lot effort has been made on analyzing misfit strain-temperature phase diagram of different ferroelectric and ferromagnetic thin films grown on substrates (Pertsev, 2008; Pertsev et al., 2003; Pertsev et al., 2000). Despite the phenomenological essence of the Landau theory, the determination of the Landau coefficients can be connected to first-principle calculation (Tagantsev, Gerra, & Setter, 2008). All these works implied great tunability of ferroelectric/ferromagnetic phases and physical properties of the thin films via changing the substrate misfit strain. Yet, the misfit strain between the thin film and the substrate is determined by the choice of materials. For given thin film and substrate, the misfit strain is usually considered constant in various theoretical models. To obtain arbitrary value of misfit strain is a rigorous requirement on material selection. An alternative approach is to consider multilayers and to control the physical properties of multilayers by adjusting the thickness ratio between different slabs. On this basis, Prokhorenko and Pertsev (2010) constructed the energy expression for free-standing ferroelectric multilayers and put forward the idea of tunable physical properties of ferroelectric multilayers by adjusting the thickness ratio between the ferroelectric slab and the passive slab.

Due to the effectiveness of phase control in ferroelectric/ferromagnetic thin films by adjusting the mechanical strains, theoretical and experimental works spring up on strain engineering of multiferroic multilayers and superlattices (Liu, Nan, Xu, & Chen, 2005; Murugavel, Padhan, & Prellier, 2004; Pertsev & Kohlstedt, 2010; Pertsev, Kohlstedt, & Dkhil, 2009; Wu et al., 2006). Multiferroic multilayers are obtained by simply replacing the passive slabs in the ferroelectric multilayers by ferromagnetic slabs. In this case, the passive slabs change into functional slabs and the product ME property depends on the thickness ratio. According to the above analysis, it is necessary to find some new adjusting mechanism for the physical properties of multiferroic multilayers. A substrate-multiferroic multilayer system provides this possibility. On one hand, substrate-induced straining and clamping provides different mechanical conditions for the multilayer without changing its microstructure; on the other hand, this clamping condition can be easily adjusted by changing the thickness ratio between the substrate and the multilayer.

In this paper, we discuss the possibility of controlling the phase diagrams and physical properties of a multiferroic multilayer sandwiched between substrates by adjusting the thickness ratio of the substrates. The total strains in different layers are first solved as functions of misfit strains, electric polarizations of the ferroelectric slabs and magnetic polarizations of the ferromagnetic slabs. Then thermodynamic potentials are constructed for ferroelectric/elastic multilayers and ferroelectric/ferromagnetic multilayers sandwiched between elastic substrates by using the solution of the strains. Using the potential for ferroelectric/ferromagnetic multilayers, the ferroelectric phase diagrams for $BaTiO_3/CoFe_2O_4$ multilayer clamped in $SrTiO_3$ substrates are studied for various conditions. The strains and electric polarizations are also plotted at room temperature as functions of the misfit strains.

2. Mechanics solution for the strains

Consider a structure illustrated in Fig. 1, h and H denote respectively the thickness of the multilayer and substrate, t_f and t_p denote respectively the thickness of the one ferroelectric slab and one passive slab (ferromagnetic slab) in the multilayer and substrate, the multilayer is composed of n ferroelectric slabs and $n+1$ passive slabs. Two thickness ratios is defined by $\lambda_1 = \frac{nt_f}{nt_f+(n+1)t_p}$ and $\lambda_2 = \frac{h}{2H+h}$, respectively. Due to symmetry property of the whole structure, in our model the bending effect is neglected. Two important assumptions are taken in the following deduction, one is the ferroelectric and ferromagnetic slabs are always in single domain state and the other is that the depolarization fields and short range interaction at the interface

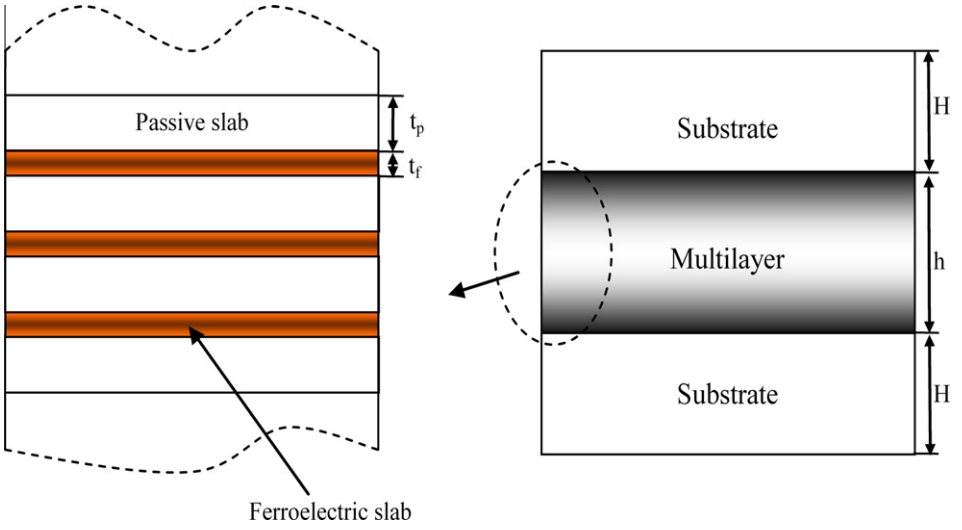

Fig. 1. Configuration of a multiferroic multilayer clamped between two substrates.

between different slabs are not considered here, the application of the second assumption to multiferroic superlattices or slabs with thickness less than 100 nm should be cautious (Prokhorenko & Pertsev, 2010).

For a free standing ferroelectric slab, the energy state is described by its electric polarizations P_i, (i = 1,2,3) and stresses σ_{ij}, (i,j = 1,2,3), and the Gibbs free energy density is given by Li, Cross, and Chen (2005)

$$\begin{aligned}
G_f = {} & \alpha_1\left(P_1^2+P_2^2+P_3^2\right)+\alpha_{11}\left(P_1^4+P_2^4+P_3^4\right)+\alpha_{12}\left(P_1^2P_2^2+P_1^2P_3^2+P_2^2P_3^2\right)+\alpha_{111}\left(P_1^6+P_2^6+P_3^6\right)\\
& +\alpha_{112}\left[P_1^4\left(P_2^2+P_3^2\right)+P_2^4\left(P_1^2+P_3^2\right)+P_3^4\left(P_1^2+P_2^2\right)\right]+\alpha_{123}P_1^2P_2^2P_3^2+\alpha_{1111}\left(P_1^8+P_2^8+P_3^8\right)\\
& +\alpha_{1112}\left[P_1^6\left(P_2^2+P_3^2\right)+P_2^6\left(P_1^2+P_3^2\right)+P_3^6\left(P_1^2+P_2^2\right)\right]+\alpha_{1122}\left(P_1^4P_2^4+P_2^4P_3^4+P_1^4P_3^4\right)\\
& +\alpha_{1123}\left(P_1^4P_2^2P_3^2+P_2^4P_1^2P_3^2+P_3^4P_1^2P_2^2\right)-\frac{s_{11}}{2}\left(\sigma_{11}^2+\sigma_{22}^2+\sigma_{33}^2\right)-s_{12}\left(\sigma_{11}\sigma_{22}+\sigma_{11}\sigma_{33}+\sigma_{22}\sigma_{33}\right)\\
& -\frac{s_{44}}{2}\left(\sigma_{23}^2+\sigma_{13}^2+\sigma_{12}^2\right)-Q_{11}\left(\sigma_{11}P_1^2+\sigma_{22}P_2^2+\sigma_{33}P_3^2\right)-Q_{44}\left(P_2P_3\sigma_{23}+P_1P_3\sigma_{13}+P_2P_1\sigma_{12}\right)\\
& -Q_{12}\left[\sigma_{11}\left(P_2^2+P_3^2\right)+\sigma_{22}\left(P_1^2+P_3^2\right)+\sigma_{33}\left(P_1^2+P_2^2\right)\right],
\end{aligned} \tag{1}$$

where α_i, α_{ij} represent the dielectric stiffness and higher-order stiffness coefficients at constant stress, s_{ij} are the elastic compliances and Q_{ij} are the electrostrictive constants. For a general plane stress condition ($\sigma_{13} = \sigma_{23} = \sigma_{33} = 0$), the strains of the ferroelectric slabs are derived by using the constitutive relations $u_{ij} = -\partial G_f/\partial\sigma_{ij}$ as

$$\begin{aligned}
u_{11} &= s_{11}\sigma_{11}+s_{12}\sigma_{22}+Q_{11}P_1^2+Q_{12}(P_2^2+P_3^2),\\
u_{22} &= s_{11}\sigma_{22}+s_{12}\sigma_{11}+Q_{11}P_2^2+Q_{12}(P_1^2+P_3^2),\\
u_{12} &= s_{44}\sigma_{12}+Q_{44}P_1P_2.\\
u_{33} &= s_{12}(\sigma_{11}+\sigma_{22})+Q_{11}P_3^2+Q_{12}\left(P_1^2+P_2^2\right),\\
u_{23} &= Q_{44}P_2P_3,\\
u_{13} &= Q_{44}P_1P_3.
\end{aligned} \tag{2}$$

The expressions of the total strains in Eq. (2) take the general form of $u_{ij} = u_{ij}^e + u_{ij}^*$, where $u_{ij}^e = u_{ij}^e(\sigma)$ denotes the elastic strains related to the stresses and $u_{ij}^* = u_{ij}^*(P)$ denotes the eigenstrains caused by paraelectric–ferroelectric phase transition. The in-plane stresses σ_{11}, σ_{22} and σ_{12} can be solved as functions of the in-plane strains u_{11}, u_{22} and u_{12} from the first three equations in Eq. (2). For a multiferroic multilayer, the ferroelectric slabs are clamped in ferromagnetic slabs (or elastic slabs for ferroelectric multilayers). Thus the boundary conditions at the interfaces of the ferroelectric slabs and ferromagnetic (or elastic) slabs are expressed by strains. And when substrates are added, the boundary conditions at the interfaces of the passive slabs and the substrates are also expressed by strains. In both cases, the energy state should be described by the Helmholtz free energy density F_f (Prokhorenko & Pertsev, 2010). F_f can be obtained from the Gibbs free energy density G_f via the inverse Legendre transformation $F_f = G_f + \sum_{j\geqslant i} u_{ij}\sigma_{ij}$. Using the in-plane strains u_{11},u_{22} and u_{12}, and electric polarizations P_1, P_2, and P_3 as its independent variables, F_f is given by Zembilgotov et al. (2005)

$$F_f = \alpha_1^* P_1^2 + \alpha_2^* P_2^2 + \alpha_3^* P_3^2 + \alpha_6^* P_1 P_2 + \alpha_{11}^* \left(P_1^4 + P_2^4\right) + \alpha_{33}^* P_3^4 + \alpha_{12}^* P_1^2 P_2^2 + \alpha_{13}^* \left(P_1^2 + P_2^2\right) P_3^2 + \alpha_{111} \left(P_1^6 + P_2^6 + P_3^6\right) + \alpha_{112} \left[P_1^4 \left(P_2^2 + P_3^2\right) + P_2^4 \left(P_1^2 + P_3^2\right) + P_3^4 \left(P_1^2 + P_2^2\right)\right] + \alpha_{123} P_1^2 P_2^2 P_3^2 + \alpha_{1111} \left(P_1^8 + P_2^8 + P_3^8\right) + \alpha_{1112} \left[P_1^6 \left(P_2^2 + P_3^2\right) + P_2^6 \left(P_1^2 + P_3^2\right) + P_3^6 \left(P_1^2 + P_2^2\right)\right] + \alpha_{1122} \left(P_1^4 P_2^4 + P_2^4 P_3^4 + P_1^4 P_3^4\right) + \alpha_{1123} \left(P_1^4 P_2^2 P_3^2 + P_2^4 P_1^2 P_3^2 + P_3^4 P_1^2 P_2^2\right) + \frac{[s_{11}(u_{11}^2 + u_{22}^2) - 2s_{12} u_{11} u_{22}]}{2(s_{11}^2 - s_{12}^2)} + \frac{u_{12}^2}{2s_{44}}, \tag{3}$$

where

$$\alpha_1^* = \alpha_1 + \frac{u_{11}(Q_{12}s_{12} - Q_{11}s_{11}) + u_{22}(Q_{11}s_{12} - Q_{12}s_{11})}{(s_{11}^2 - s_{12}^2)},$$
$$\alpha_2^* = \alpha_1 + \frac{u_{22}(Q_{12}s_{12} - Q_{11}s_{11}) + u_{11}(Q_{11}s_{12} - Q_{12}s_{11})}{(s_{11}^2 - s_{12}^2)}, \tag{4}$$
$$\alpha_3^* = \alpha_1 - \frac{Q_{12}(u_{11} + u_{22})}{(s_{11} + s_{12})}, \alpha_6^* = -\frac{Q_{44}}{s_{44}} u_{12},$$

and α_{ij}^* can be obtained from the classic work on thermodynamics of ferroelectric thin films (Pertsev et al., 1998).

First, we consider the passive slab to be made up of linear elastic materials, and their elastic strains are denoted by v_{ij}. For a dislocation-free interface between the ferroelectric slab and the passive slab, the in-plane strains in the two kinds of slabs satisfy

$$v_{11} = u_{11} - u_{m1}^p, \ v_{22} = u_{22} - u_{m2}^p, \ v_{12} = u_{12} - u_{m6}^p, \tag{5}$$

where u_{m1}^p, u_{m2}^p and u_{m6}^p are the misfit strains between the ferroelectric slab and the passive slab. As shown in Fig. 1, the multilayer is clamped in substrates, which gives

$$w_{11} = v_{11} - u_{m1}^s, \ w_{22} = v_{22} - u_{m2}^s, \ w_{12} = v_{12} - u_{m6}^s, \tag{6}$$

where w_{ij} denotes the elastic strains of the substrate layer, u_{m1}^s, u_{m2}^s and u_{m6}^s are the misfit strains between the passive slab and the elastic substrate. Assume that the solution for the strains are independent of the out-of-plane axis x_3, the total stresses acting on the surface section perpendicular to x_1 and x_2 axes should vanish, which gives

$$\begin{aligned} &\lambda_1\lambda_2\sigma_{11} + (1-\lambda_1)\lambda_2\sigma_{11}^p + (1-\lambda_2)\sigma_{11}^s = 0, \\ &\lambda_1\lambda_2\sigma_{22} + (1-\lambda_1)\lambda_2\sigma_{22}^p + (1-\lambda_2)\sigma_{22}^s = 0, \\ &\lambda_1\lambda_2\sigma_{12} + (1-\lambda_1)\lambda_2\sigma_{12}^p + (1-\lambda_2)\sigma_{12}^s = 0, \end{aligned} \tag{7a – c}$$

where σ_{ij}^p and σ_{ij}^s denote respectively the elastic stress in the passive slab and the substrate. Since $\sigma_{ij} = \frac{\partial F_f}{\partial u_{ij}}$, $\sigma_{ij}^p = \frac{\partial F_p}{\partial v_{ij}}$, $\sigma_{ij}^s = \frac{\partial F_s}{\partial w_{ij}}$, where F_p and F_s denote respectively the Helmholtz free energy density of the passive slabs, and the substrate, Eq. (7a–c) can also be expressed as

$$\begin{aligned} &\lambda_1\lambda_2 \frac{\partial F_f}{\partial u_{11}} + (1-\lambda_1)\lambda_2 \frac{\partial F_p}{\partial v_{11}} + (1-\lambda_2)\frac{\partial F_s}{\partial w_{11}} = 0, \\ &\lambda_1\lambda_2 \frac{\partial F_f}{\partial u_{22}} + (1-\lambda_1)\lambda_2 \frac{\partial F_p}{\partial v_{22}} + (1-\lambda_2)\frac{\partial F_s}{\partial w_{22}} = 0, \\ &\lambda_1\lambda_2 \frac{\partial F_f}{\partial u_{12}} + (1-\lambda_1)\lambda_2 \frac{\partial F_p}{\partial v_{12}} + (1-\lambda_2)\frac{\partial F_s}{\partial w_{12}} = 0, \end{aligned} \tag{8a – c}$$

First consider the case when the passive slabs are made up of elastic materials, we have

$$F_p = \frac{1}{2} c_{11}^p (v_{11}^2 + v_{22}^2 + v_{33}^2) + c_{12}^p (v_{11} v_{22} + v_{11} v_{33} + v_{22} v_{33}) + \frac{1}{2} c_{44}^p (v_{12}^2 + v_{23}^2 + v_{13}^2), \tag{9}$$

where c_{ij}^p are the elastic stiffness constants and v_{ij} are the strains for the elastic passive slabs.

For elastic substrate, we have

$$F_s = \frac{1}{2} c_{11}^s (w_{11}^2 + w_{22}^2 + w_{33}^2) + c_{12}^s (w_{11} w_{22} + w_{11} w_{33} + w_{22} w_{33}) + \frac{1}{2} c_{44}^w (w_{12}^2 + w_{23}^2 + w_{13}^2), \tag{10}$$

where c_{ij}^s are the elastic stiffness constants and w_{ij} are the strains for the substrate layer.

Substituting Eqs. (3), (9), (10) into Eq. (8), we can solve u_{ij} as functions of the electric polarizations P_i, and the misfit strains $u_{m1}^p, u_{m2}^p, u_{m6}^p$ and $u_{m1}^s, u_{m2}^s, u_{m6}^s$. For isotropic in-plane misfit strains $u_{m1}^p = u_{m2}^p = u_m^p$, $u_{m6}^p = 0$, $u_{m1}^s = u_{m2}^s = u_m^s$, $u_{m6}^s = 0$, the solution is given by

$$u_{11} = \frac{1}{1+b_1+b_2}\left[\frac{1}{2}(Q_{11}+Q_{12})\left(P_1^2+P_2^2\right)+Q_{12}P_3^2+(b_1+b_2)u_m^p+b_2u_m^s\right]+\frac{(Q_{11}-Q_{12})}{2(1+b_4+b_5)}\left(P_1^2-P_2^2\right),$$
$$u_{22} = \frac{1}{1+b_1+b_2}\left[\frac{1}{2}(Q_{11}+Q_{12})\left(P_1^2+P_2^2\right)+Q_{12}P_3^2+(b_1+b_2)u_m^p+b_2u_m^s\right]-\frac{(Q_{11}-Q_{12})}{2(1+b_4+b_5)}\left(P_1^2-P_2^2\right), \quad (11a-c)$$
$$u_{12} = \frac{Q_{44}}{b_3}P_1P_2,$$

where

$$b_1 = \frac{(1-\lambda_1)(s_{11}+s_{12})}{\lambda_1\left(s_{11}^p+s_{12}^p\right)},\ b_2 = \frac{(1-\lambda_2)(s_{11}+s_{12})}{\lambda_1\lambda_2\left(s_{11}^s+s_{12}^s\right)},\ b_3 = 1+\frac{(1-\lambda_1)s_{44}}{\lambda_1 s_{44}^p}+\frac{(1-\lambda_2)s_{44}}{\lambda_1\lambda_2 s_{44}^s},$$
$$b_4 = \frac{(1-\lambda_1)(s_{11}-s_{12})}{\lambda_1\left(s_{11}^p-s_{12}^p\right)},\ b_5 = \frac{(1-\lambda_2)(s_{11}-s_{12})}{\lambda_1\lambda_2\left(s_{11}^s-s_{12}^s\right)}. \quad (12)$$

In Eqs. (11) and (12), s_{ij}^p and s_{ij}^s denote the elastic compliances for the passive slab and the substrate, respectively.

If the passive slab is made up of ferromagnetic materials, its Helmholtz free energy density F_p takes the form Bichurin, Petrov, Ryabkov, Averkin, and Srinivasan (2005)

$$F_p = -\mathbf{M}\times\mathbf{H}_i+\frac{K_1}{M_s^4}\left(M_1^2M_2^2+M_2^2M_3^2+M_1^2M_3^2\right)+\frac{B_1}{M_s^2}\left(M_1^2v_{11}+M_2^2v_{22}+M_3^2v_{33}\right)+\frac{B_2}{M_s^2}(M_1M_2v_{12}+M_2M_3v_{23}$$
$$+M_1M_3v_{13})+\frac{1}{2}c_{11}^p(v_{11}^2+v_{22}^2+v_{33}^2)+c_{12}^p(v_{11}v_{22}+v_{11}v_{33}+v_{22}v_{33})+\frac{1}{2}c_{44}^p(v_{12}^2+v_{23}^2+v_{13}^2), \quad (13)$$

where $\mathbf{M}$ is the magnetization vector and $\mathbf{H}_i$ is the vector of the internal magnetic field, K_1 is the cubic anisotropy constant and M_s is the saturation magnetization, B_1 and B_2 denote the magnetoelastic coefficients. By using Eq. (13) instead of (9), the in-plane strains in the ferroelectric slabs are recasted as

$$u_{11} = \frac{1}{1+b_1+b_2}\left[\frac{1}{2}(Q_{11}+Q_{12})\left(P_1^2+P_2^2\right)+Q_{12}P_3^2+(b_1+b_2)u_m^p+b_2u_m^s+b_1s_{12}^pB_1\frac{M_3^2}{M_s^2}+b_1\frac{s_{11}^p+s_{12}^p}{2}B_1\frac{M_1^2+M_2^2}{M_s^2}\right]$$
$$+\frac{1}{2(1+b_4+b_5)}\left[(Q_{11}-Q_{12})\left(P_1^2-P_2^2\right)+b_4\left(s_{11}^p-s_{12}^p\right)B_1\frac{M_1^2-M_2^2}{M_s^2}\right],$$
$$u_{22} = \frac{1}{1+b_1+b_2}\left[\frac{1}{2}(Q_{11}+Q_{12})\left(P_1^2+P_2^2\right)+Q_{12}P_3^2+(b_1+b_2)u_m^p+b_2u_m^s+b_1s_{12}^pB_1\frac{M_3^2}{M_s^2}+b_1\frac{s_{11}^p+s_{12}^p}{2}B_1\frac{M_1^2+M_2^2}{M_s^2}\right]$$
$$-\frac{1}{2(1+b_4+b_5)}\left[(Q_{11}-Q_{12})\left(P_1^2-P_2^2\right)+b_4\left(s_{11}^p-s_{12}^p\right)B_1\frac{M_1^2-M_2^2}{M_s^2}\right],$$
$$u_{12} = \frac{Q_{44}}{b_3}P_1P_2-\frac{(1-\lambda_1)B_2s_{44}M_1M_2}{b_3\lambda_1M_s^2}. \quad (14a-c)$$

Substitution of Eq. (14a–c) or Eq. (11a–c) into Eqs. (5) and (6) yields the corresponding solution for $v_{ij}$and w_{ij}.

3. Energy formulation

Let us consider the total energy of the structure illustrated in Fig. 1, under the straining condition, the total energy of the system should be described by its Helmholtz free energy density, which is given by

$$\langle F\rangle = \lambda_1\lambda_2F_f+(1-\lambda_1)\lambda_2F_p+(1-\lambda_2)F_s, \quad (15)$$

where

$$\lambda_1 = \frac{nt_f}{nt_f+(n+1)t_p},\ \lambda_2 = \frac{h}{2H+h}, \quad (16)$$

n denotes the number of the ferroelectric slabs in the multilayer.

The Helmholtz free energy density of the substrate-multilayer-substrate system then obtained by substituting corresponding expressions into Eq. (15) as

$$\begin{aligned}\langle F\rangle = {} & \alpha_1^{**}\left(P_1^2+P_2^2\right)+\alpha_3^{**}P_3^2+\alpha_{11}^{**}\left(P_1^4+P_2^4\right)+\alpha_{33}^{**}P_3^4+\alpha_{12}^{**}P_1^2P_2^2+\alpha_{13}^{**}\left(P_1^2+P_2^2\right)P_3^2+\lambda_1\lambda_2\alpha_{111}\left(P_1^6+P_2^6+P_3^6\right)\\ & +\lambda_1\lambda_2\alpha_{112}\left[P_1^4\left(P_2^2+P_3^2\right)+P_2^4\left(P_1^2+P_3^2\right)+P_3^4\left(P_1^2+P_2^2\right)\right]+\lambda_1\lambda_2\alpha_{123}P_1^2P_2^2P_3^2+\lambda_1\lambda_2\alpha_{1111}\left(P_1^8+P_2^8+P_3^8\right)\\ & +\lambda_1\lambda_2\alpha_{1112}\left[P_1^6\left(P_2^2+P_3^2\right)+P_2^6\left(P_1^2+P_3^2\right)+P_3^6\left(P_1^2+P_2^2\right)\right]+\lambda_1\lambda_2\alpha_{1122}\left(P_1^4P_2^4+P_2^4P_3^4+P_1^4P_3^4\right)\\ & +\lambda_1\lambda_2\alpha_{1123}\left(P_1^4P_2^2P_3^2+P_2^4P_1^2P_3^2+P_3^4P_1^2P_2^2\right)+\langle F_0\rangle,\end{aligned} \tag{17}$$

where $\langle F_0\rangle$ denotes the part of energy that is independent on the electric polarizations, and other coefficients are given in Appendix A.

When $\lambda_2 = 1$, the substrate-multilayer-substrate system reduces to a free-standing multilayer, and the energy density expression in Eq. (17) is equivalent to the result obtained by Prokhorenko and Pertsev (2010).

If the passive slab is made up of ferromagnetic materials, Eq. (13) should be used instead of Eq. (9). The average Helmholtz free energy density of the substrate-multilayer-substrate system is reconstructed as

$$\begin{aligned}\langle F^*\rangle = {} & \alpha_1^{***}P_1^2+\alpha_2^{***}P_2^2+\alpha_3^{***}P_3^2+\alpha_6^{***}P_1P_2+\alpha_{11}^{**}\left(P_1^4+P_2^4\right)+\alpha_{33}^{**}P_3^4+\alpha_{12}^{**}P_1^2P_2^2+\alpha_{13}^{**}\left(P_1^2+P_2^2\right)P_3^2\\ & +\lambda_1\lambda_2\alpha_{111}\left(P_1^6+P_2^6+P_3^6\right)+\lambda_1\lambda_2\alpha_{112}\left[P_1^4\left(P_2^2+P_3^2\right)+P_2^4\left(P_1^2+P_3^2\right)+P_3^4\left(P_1^2+P_2^2\right)\right]+\lambda_1\lambda_2\alpha_{123}P_1^2P_2^2P_3^2\\ & +\lambda_1\lambda_2\alpha_{1111}\left(P_1^8+P_2^8+P_3^8\right)+\lambda_1\lambda_2\alpha_{1112}\left[P_1^6\left(P_2^2+P_3^2\right)+P_2^6\left(P_1^2+P_3^2\right)+P_3^6\left(P_1^2+P_2^2\right)\right]\\ & +\lambda_1\lambda_2\alpha_{1122}\left(P_1^4P_2^4+P_2^4P_3^4+P_1^4P_3^4\right)+\lambda_1\lambda_2\alpha_{1123}\left(P_1^4P_2^2P_3^2+P_2^4P_1^2P_3^2+P_3^4P_1^2P_2^2\right)+\langle F_M^*\rangle+\langle F_0^*\rangle,\end{aligned} \tag{18}$$

where the expressions for coefficients are given in Appendix A.

For practical consideration, the magnetic polarizations are always poled in certain direction to its saturation value to increase the magnetostriction effect. This is due to the fact that compared with the electrostriction effect in the ferroelectric materials the magnetoelastic effect is weak when the magnetization is far away from its saturation value. In this case, Eq. (18) can be used to analysis the ferroelectric phase diagram of the multiferroic multilayer.

4. Phase diagrams

By using Eqs. (17) and (18), the phase diagrams for ferroelectric multilayer and multiferroic multilayer controlled by compliant substrates can be plotted. From the energy expressions we can see coupling effect of factors such as misfit strains between the substrate and the multilayer, misfit strains within the multilayer, thickness ratio λ_1 and λ_2, and for multiferroic multilayer the direction of the magnetization in the ferromagnetic slab. In order to illustrate the effects of these factors, four groups of phase diagrams are plotted for $BaTiO_3$–$CoFe_2O_4$ multilayer clamped by $SrTiO_3$ substrate. The material parameters are listed in Table 1.

First we could like to discuss the effect of magnetization on the phase diagrams and to check our calculation programs. In Fig. 2, phase diagram was plotted with $\lambda_2 = 1,\ u_m^p = 0.5\times10^{-3},\ \lambda_1 \in (0, 1)$ for $BaTiO_3$-$CoFe_2O_4$ multilayer, and the $CoFe_2O_4$ slab is treated respectively as elastic material (dashed lines) and as ferromagnetic material poled in x_3 axis (solid lines). The dashed lines give the same result with Fig. 5. in Prokhorenko and Pertsev's work (Prokhorenko & Pertsev, 2010). In Fig. 2, the

Table 1
Material parameters used in calculation.

$BaTiO_3$
Landau coefficients (Li et al., 2005): $a_1 = 4.124\times10^5\ (T-115)\ (C^{-2}\,m^2\,N)$; $a_{11} = -2.097\times10^8\ (C^{-4}\,m^6\,N)$; $a_{12} = 7.974\times10^8\ (C^{-4}\,m^6\,N)$; $a_{111} = 1.294\times10^9\ (C^{-6}\,m^{10}\,N)$; $a_{112} = -1.950\times10^9\ (C^{-6}\,m^{10}\,N)$; $a_{123} = -2.5\times10^9\ (C^{-6}\,m^{10}\,N)$; $a_{1111} = 3.863\times10^{10}\ (C^{-6}\,m^{10}\,N)$; $a_{1112} = 2.529\times10^{10}\ (C^{-6}\,m^{10}\,N)$; $a_{1122} = 1.637\times10^{10}\ (C^{-6}\,m^{10}\,N)$; $a_{1123} = 1.367\times10^{10}\ (C^{-6}\,m^{10}\,N)$; *Electrostrictive coefficients* (Pertsev et al., 1998): $Q_{11} = 0.11, Q_{12} = -0.043, Q_{44} = 0.059\ (C^{-1}m^2)$;
Elastic constants (Pertsev et al., 1998): $s_{11} = 8.3\times10^{-12}\ (N^{-1}\,m^2)$; $s_{12} = -2.7\times10^{-12}\ (N^{-1}\,m^2)$; $s_{44} = 9.24\times10^{-12}\ (N^{-1}\,m^2)$
$CoFe_2O_4$
Elastic constants (Prokhorenko & Pertsev, 2010): $s_{11}^p = 6.427\times10^{-12}\ (N^{-1}\,m^2)$; $s_{12}^p = -2.422\times10^{-12}\ (N^{-1}\,m^2)$; $s_{44}^p = 2.222\times10^{-11}\ (N^{-1}\,m^2)$
Magnetic properties (Pertsev, 2008): $M_s = 3.5\times10^5 (Am^{-1})$; $B_1 = 5.9\times10^7\ (J/m^3)$
$SrTiO_3$(Pertsev et al., 2000): $s_{11}^s = 3.296\times10^{-12}\ (N^{-1}\,m^2)$; $s_{12}^s = -0.736\times10^{-12}\ (N^{-1}\,m^2)$; $s_{44}^s = 7.813\times10^{-12}\ (N^{-1}\,m^2)$

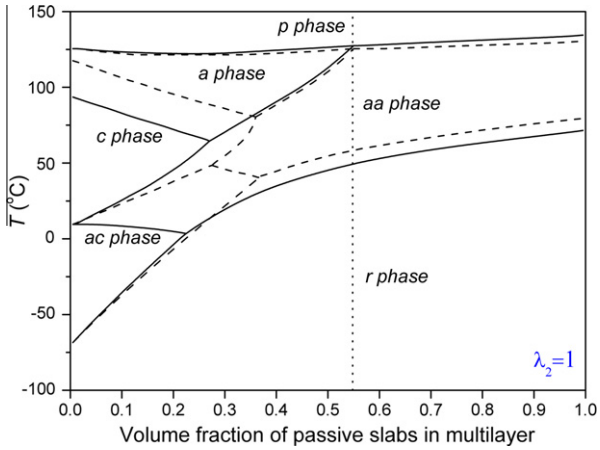

Fig. 2. Volume fraction of passive slab-temperature phase diagram of BTO multilayer with $u_m^p = 0.5 \times 10^{-3}$ for elastic CFO passive slab (dashed lines), and for ferromagnetic CFO passive slab (solid lines).

phase diagrams present gradual change of physical properties of the ferroelectric slab from bulk materials (left) to thin films on thick substrate (right). A threshold volume fraction λ_1^0 exists as a function of λ_2 (or λ_2^0 as a function of λ_1), above which the

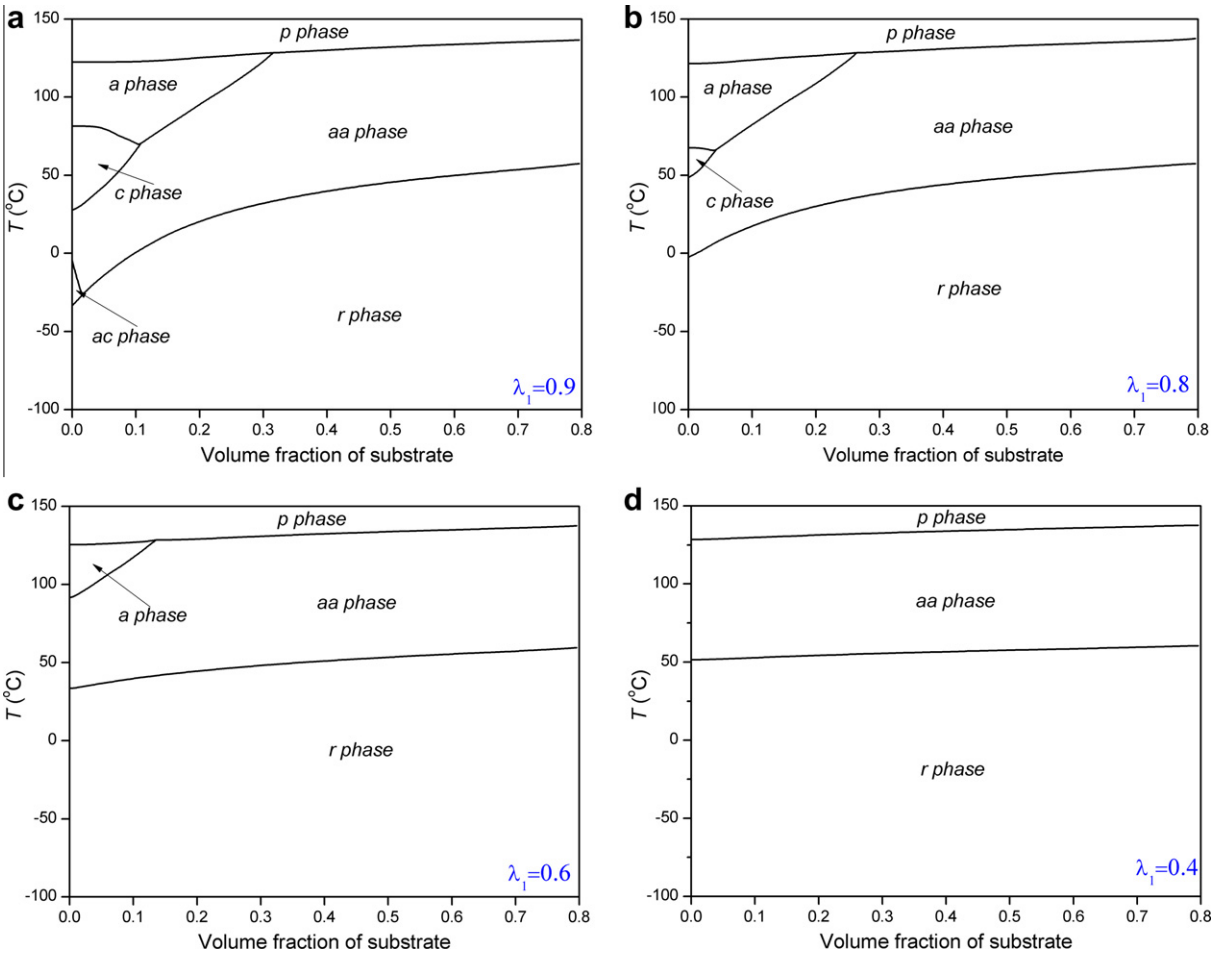

Fig. 3. Volume fraction of substrate-temperature phase diagram of BTO ferroelectric multilayer with $u_m^p = 0.5 \times 10^{-3}$, $u_m^s = 0.3 \times 10^{-3}$ for (a) $\lambda_1 = 0.9$, (b) $\lambda_1 = 0.8$, (c) $\lambda_1 = 0.6$, (d) $\lambda_1 = 0.4$.

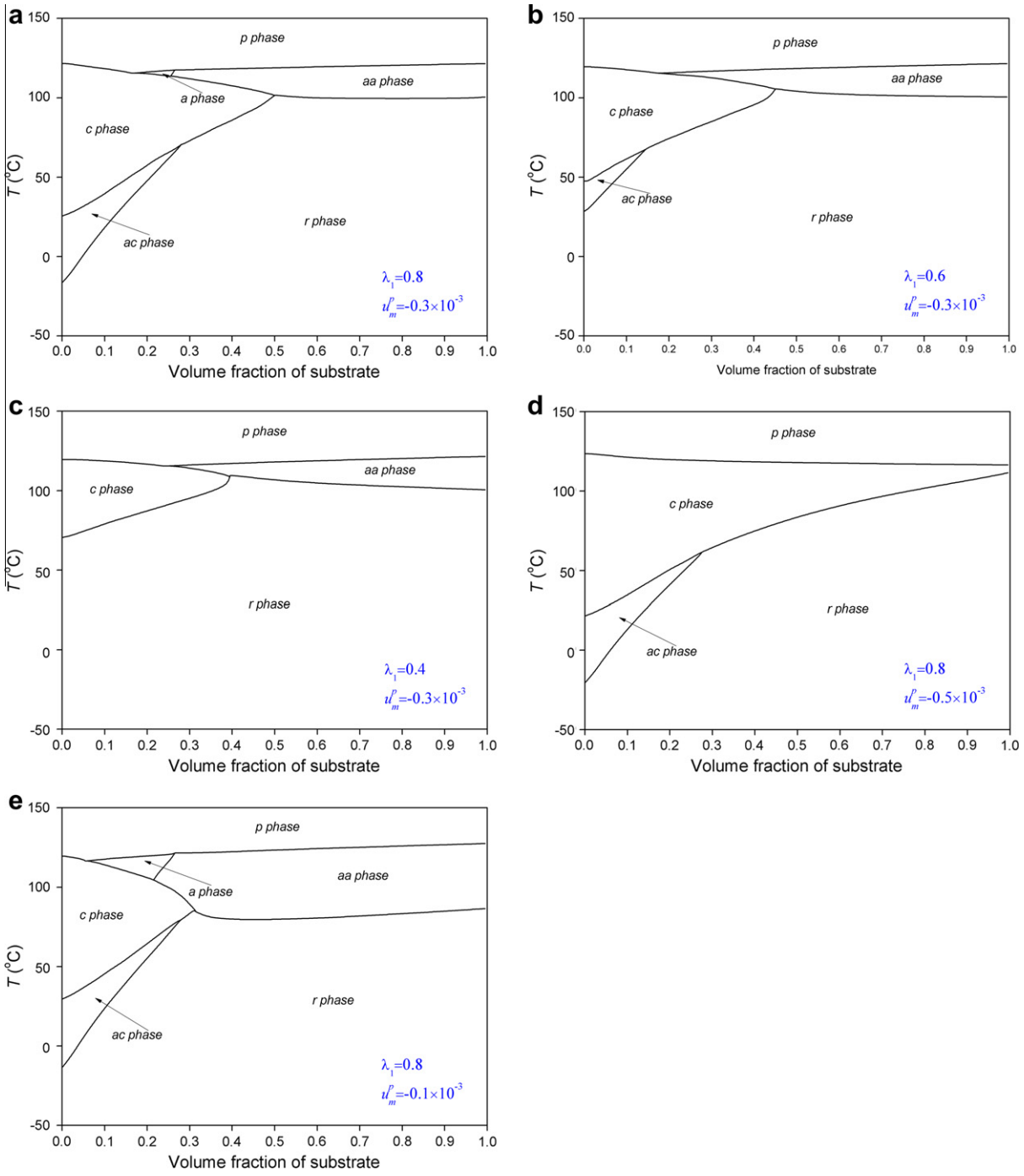

Fig. 4. Volume fraction of substrate-temperature phase diagram of BTO-CFO multiferroic multilayer with $u_m^p = -0.3 \times 10^{-3}$, $u_m^s = 0.5 \times 10^{-3}$ for (a) $\lambda_1 = 0.8$, (b) $\lambda_1 = 0.6$, (c) $\lambda_1 = 0.4$; and with $u_m^s = 0.5 \times 10^{-3}$, $\lambda_1 = 0.8$ for (d) $u_m^p = -0.5 \times 10^{-3}$, (e) $u_m^p = -0.1 \times 10^{-3}$.

diagram becomes qualitatively similar to that of a thin film. For both dashed lines and solid lines, this threshold volume fraction $\lambda_1^0(\lambda_2 = 1) = 0.548$. The equivalence is due to the fact that addition of the magnetization merely renormalizes the second-order coefficients a_i^{***} while the threshold volume fraction is solved from the equation $a_{11}^{**} = a_{12}^{**}/2$.

The main purpose of our following calculation is to examine the effect of adjustable substrate on the phase diagrams and hence physical properties of the multiferroic composites. From Fig. 3(a) to (d), we illustrate that by adjusting the volume fraction of the substrate ($l = 1 - \lambda_2$), the phase diagrams of the multilayer can be controlled in similar way as adjusting the volume fraction of the passive slab. Moreover, we show that for different values of λ_1 the appearance of certain phases

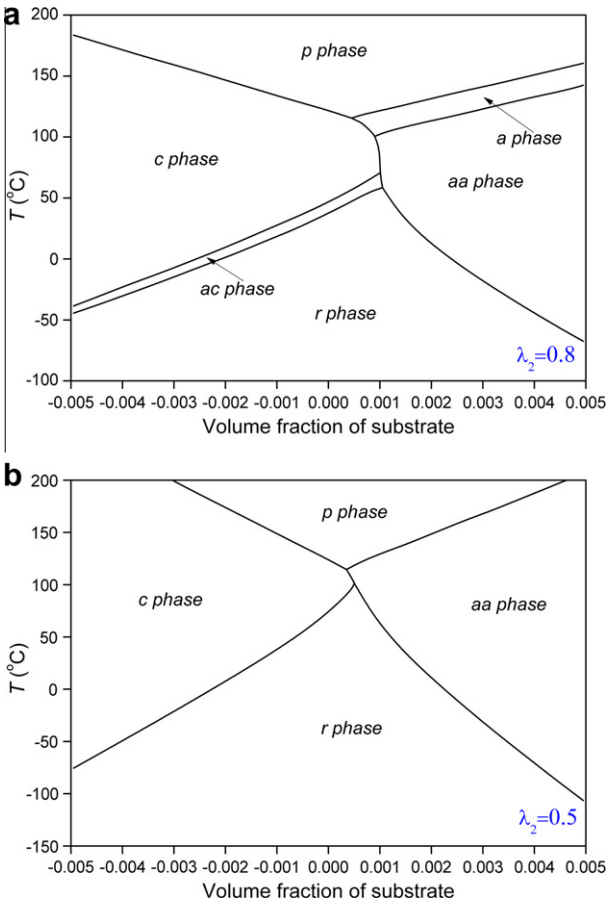

Fig. 5. Pertsev misfit-temperature phase diagram of BTO-CFO multiferroic multilayer with $\lambda_1 = 0.8$, $u_m^p = -0.3 \times 10^{-3}$, $u_m^s = 0.5 \times 10^{-3}$ for (a) $\lambda_2 = 0.8$, (b) $\lambda_2 = 0.5$.

in the diagram is tunable. In Fig. 3(a) the appeared phases are the same with the phases in Fig. 2. In Fig. 3(b–d) *ac phase*, *c phase* and *a phase* disappear in succession. It is clear seen from the phase diagrams that the tunability of the stabilized phases and hence physical properties is greatly enhanced by introducing the finite thickness substrate.

To further investigate the tunability of phase diagrams, we calculate the case when the misfit strains in substrate and passive slabs take different signs in Fig. 4. In Fig. 4, *l*-temperature phase diagrams are plotted with different signs of u_m^p and u_m^s. Since u_m^p and u_m^s take different signs, the clamping condition of the passive slab is weaken by the presence of the substrate, which causes different configuration of the phase diagrams. In Fig. 4, a general character of the phase diagrams is that *c phase* is greatly strengthened due to minus u_m^p, and a new triple point appears, corresponding to λ_2^0, separating *c phase*, *aa phase*, and *r phase*. In Fig. 4(a–c), the calculation was done for increasing volume fraction of the substrate. From the results we can conclude that by adjusting the volume fraction of the substrate, the presence of *a phase* and *ac phase* is tunable, and the value of λ_2^0 is slightly affected. In Fig. 4(a, d, e), the calculation was done for different values of u_m^p, which shows that λ_2^0 depends strongly on u_m^p.

Finally, the traditional misfit strain u_m^s-temperature phase diagrams are plotted with different values of λ_2, from which we can see the effect of adjusting substrate thickness on the Pertsev diagram. It is shown in Fig. 5 that by adjusting λ_2, the presence of the intermediate *a phase* and *ac phase* can be controlled.

5. In-plane strains of the ferroelectric slabs

The change of ferroelectric states in a substrate-multiferroic multilayer system derives from the mechanical coupling at different interfaces. On the other hand, the change of the ferroelectric states (electric polarizations) in turn has an impact on the strains in different layers, as seen in Eqs. (11a–c) and (14a–c). In this section we calculate the change of in-plane strains and corresponding electric polarizations of the ferroelectric slabs at room temperature by adjusting the volume fraction of the substrate. From Eq. (2) it is shown that the total strains are made up of two parts $u_{ij} = u_{ij}^e + u_{ij}^*$. Thus we have for multiferroic multilayers

$$
\begin{aligned}
u_{11}^{e} &= \frac{1}{1+b_1+b_2}\left[\frac{1}{2}(Q_{11}+Q_{12})\left(P_1^2+P_2^2\right)+Q_{12}P_3^2+(b_1+b_2)u_m^p+b_2u_m^s+b_1s_{12}^pB_1\frac{M_3^2}{M_s^2}+b_1\frac{s_{11}^p+s_{12}^p}{2}B_1\frac{M_1^2+M_2^2}{M_s^2}\right]\\
&\quad+\frac{1}{2(1+b_4+b_5)}\left[(Q_{11}-Q_{12})\left(P_1^2-P_2^2\right)+b_4(s_{11}^p-s_{12}^p)B_1\frac{M_1^2-M_2^2}{M_s^2}\right]-Q_{11}P_1^2-Q_{12}\left(P_2^2+P_3^2\right),\\
u_{22}^{e} &= \frac{1}{1+b_1+b_2}\left[\frac{1}{2}(Q_{11}+Q_{12})\left(P_1^2+P_2^2\right)+Q_{12}P_3^2+(b_1+b_2)u_m^p+b_2u_m^s+b_1s_{12}^pB_1\frac{M_3^2}{M_s^2}+b_1\frac{s_{11}^p+s_{12}^p}{2}B_1\frac{M_1^2+M_2^2}{M_s^2}\right]\\
&\quad-\frac{1}{2(1+b_4+b_5)}\left[(Q_{11}-Q_{12})\left(P_1^2-P_2^2\right)+b_4(s_{11}^p-s_{12}^p)B_1\frac{M_1^2-M_2^2}{M_s^2}\right]-Q_{11}P_2^2-Q_{12}\left(P_1^2+P_3^2\right),\\
u_{22}^{e} &= \frac{Q_{44}}{b_3}P_1P_2-\frac{(1-\lambda_1)B_2s_{44}M_1M_2}{b_3\lambda_1M_s^2}-Q_{44}P_1P_2.
\end{aligned}
\tag{19}
$$

The in-plane axial strains for the ferroelectric slabs as a function of the volume fraction of the substrate are plotted in Fig. 6(a) and (b), where the misfit strains caused by the passive slabs and the substrates takes the same (positive) sign in Fig. 6(a) and different signs in Fig. 6(b). In Fig. 6, total strains and elastic strains are illustrated with solid lines and dashed lines, respectively. The distance between the two sorts of lines corresponds to the absolute value of the eigenstrain caused by phase transition, where solid above dashed lines indicates positive eigenstrain and dashed above solid lines indicates negative eigenstrain. From Fig. 6, we can see that phase transition leads to significant changes of the in-plane strains, which derives from the change of eigenstrain caused by phase transition. From Eq. (2) and corresponding values of Q_{ij}, we learn that the eigenstrain caused by in-plane electric polarizations is positive while the eigenstrain caused by out of plane electric polarizations is negative. This explains why in Fig. 6(a) the phase transition strain decreases in a phase transition from *aa*

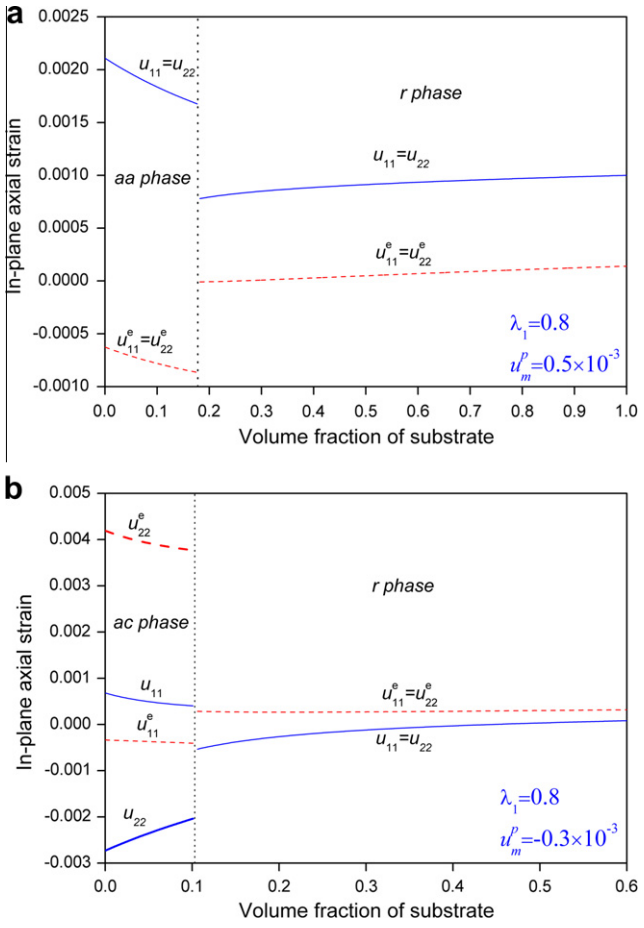

Fig. 6. In-plane axial strain in ferroelectric slabs versus volume fraction of substrate $(\lambda_1 = 0.8, u_m^s = 0.5\times10^{-3})$ for (a) $u_m^p = 0.5\times10^{-3}$, (b) $u_m^p = -0.3\times10^{-3}$.

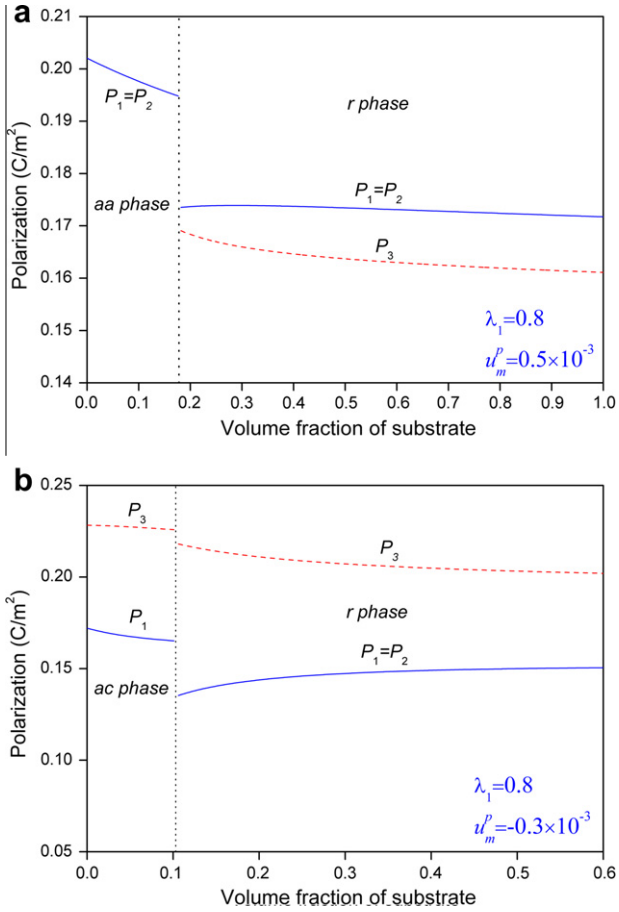

Fig. 7. Polarizations in ferroelectric slabs versus volume fraction of substrate ($\lambda_1 = 0.8, u_m^s = 0.5 \times 10^{-3}$) for (a) $u_m^p = 0.5 \times 10^{-3}$, (b) $u_m^p = -0.3 \times 10^{-3}$.

phase to *r phase*. When the ferroelectric slabs stabilize in a phase that possesses asymmetric in-plane polarization (e.g. *ac phase* in Fig. 6(b)), great anisotropy of in-plane axial strains will be generated, as presented in Fig. 6(b).

The electric polarizations of the ferroelectric slabs corresponding to Fig. 6(a) and (b) are plotted in Fig. 7(a) and (b). Compare Fig. 6 with Fig. 7, we can see that the distance between $u_{11} = u_{22}$ and $u_{11}^e = u_{22}^e$ in Fig. 6 depends on the distance between $P_1 = P_2$ and P_3. In the *r phase* section of Fig. 6(a) and (b), $u_{11} = u_{22}$ and $u_{11}^e = u_{22}^e$ switch positions with each other, while corresponding switching happens between $P_1 = P_2$ and P_3 in Fig. 7(a) and (b).

6. Conclusion

In this paper, we have comprehensively examined the tunability of the phase diagrams and physical properties of a substrate-multiferroic multilayer-substrate structure by adjusting the substrate thickness. The formulation is based on a thermodynamic potential derived from Landau-type expansion and mechanics solution of the total strains. From the results we can see that by changing the substrate thickness, the phase diagrams and physical properties can by effectively controlled. By combination with other tunable variables, transformation of the phase diagram configuration can be realized: when the misfit strains corresponding to the two kinds of interfaces take same or opposite signs, the phase diagram patterns are significantly different. The in-plane total strains and elastic strains of the ferroelectric slab take dramatic jumps at the ferroelectric phase transition point.

Acknowledgement

The work was supported by the NSFC (National Natural Science Foundation of China) through the funds (10732100, 10831160504, 10972239, 10902128), the Fundamental Research Funds for the Central Universities.

Appendix A. Coefficients in the energy formulation

The coefficients in Eq. (17) are expanded as

$$
\begin{aligned}
\alpha_1^{**} &= \lambda_1\lambda_2\alpha_1 + \frac{(Q_{11}+Q_{12})}{(1+b_1+b_2)^2}\left\{-\lambda_1\lambda_2\frac{(b_1+b_2)\left[(b_1+b_2)u_m^p+b_2u_m^s\right]}{s_{11}+s_{12}}\right.\\
&\left.+(1-\lambda_1)\lambda_2\frac{\left[-u_m^p+b_2u_m^s\right]}{s_{11}^p+s_{12}^p}+(1-\lambda_2)\frac{\left[-u_m^p-(b_1+1)u_m^s\right]}{s_{11}^s+s_{12}^s}\right\},\\
\alpha_3^{**} &= \lambda_1\lambda_2\alpha_1 + \frac{2Q_{12}}{(1+b_1+b_2)^2}\left\{-\lambda_1\lambda_2\frac{(b_1+b_2)\left[(b_1+b_2)u_m^p+b_2u_m^s\right]}{s_{11}+s_{12}}\right.\\
&\left.+(1-\lambda_1)\lambda_2\frac{\left[-u_m^p+b_2u_m^s\right]}{s_{11}^p+s_{12}^p}+(1-\lambda_2)\frac{\left[-u_m^p-(b_1+1)u_m^s\right]}{s_{11}^s+s_{12}^s}\right\},\\
\alpha_{11}^{**} &= \lambda_1\lambda_2\alpha_{11}^{*} + \frac{(Q_{11}+Q_{12})^2}{4(1+b_1+b_2)^2}\left\{-\lambda_1\lambda_2\frac{(1+2b_1+2b_2)}{s_{11}+s_{12}}+\frac{(1-\lambda_1)\lambda_2}{s_{11}^p+s_{12}^p}+\frac{(1-\lambda_2)}{s_{11}^s+s_{12}^s}\right\}\\
&+\frac{(Q_{11}-Q_{12})^2}{4(1+b_4+b_5)^2}\left\{-\lambda_1\lambda_2\frac{(1+2b_4+2b_5)}{s_{11}-s_{12}}+\frac{(1-\lambda_1)\lambda_2}{s_{11}^p-s_{12}^p}+\frac{(1-\lambda_2)}{s_{11}^s-s_{12}^s}\right\},\\
\alpha_{33}^{**} &= \lambda_1\lambda_2\alpha_{33}^{*} + \frac{Q_{12}^2}{(1+b_1+b_2)^2}\left\{-\lambda_1\lambda_2\frac{(1+2b_1+2b_2)}{s_{11}+s_{12}}+\frac{(1-\lambda_1)\lambda_2}{s_{11}^p+s_{12}^p}+\frac{(1-\lambda_2)}{s_{11}^s+s_{12}^s}\right\},\\
\alpha_{13}^{**} &= \lambda_1\lambda_2\alpha_{13}^{*} + \frac{Q_{12}(Q_{11}+Q_{12})}{(1+b_1+b_2)^2}\left\{-\lambda_1\lambda_2\frac{(1+2b_1+2b_2)}{s_{11}+s_{12}}+\frac{(1-\lambda_1)\lambda_2}{s_{11}^p+s_{12}^p}+\frac{(1-\lambda_2)}{s_{11}^s+s_{12}^s}\right\},\\
\alpha_{12}^{**} &= \lambda_1\lambda_2\alpha_{12}^{*} + \frac{(Q_{11}+Q_{12})^2}{2(1+b_1+b_2)^2}\left\{-\lambda_1\lambda_2\frac{(1+2b_1+2b_2)}{s_{11}+s_{12}}+\frac{(1-\lambda_1)\lambda_2}{s_{11}^p+s_{12}^p}+\frac{(1-\lambda_2)}{s_{11}^s+s_{12}^s}\right\}\\
&-\frac{(Q_{11}-Q_{12})^2}{2(1+b_4+b_5)^2}\left\{-\lambda_1\lambda_2\frac{(1+2b_4+2b_5)}{s_{11}-s_{12}}+\frac{(1-\lambda_1)\lambda_2}{s_{11}^p-s_{12}^p}+\frac{(1-\lambda_2)}{s_{11}^s-s_{12}^s}\right\}\\
&+\frac{Q_{44}^2}{2b_3^2}\left\{-\lambda_1\lambda_2\frac{2b_3-1}{s_{44}}+\frac{(1-\lambda_1)\lambda_2}{s_{44}^p}+\frac{(1-\lambda_2)}{s_{44}^s}\right\},
\end{aligned}
\tag{A1}
$$

The coefficients in Eq. (18) are expanded as

$$
\begin{aligned}
\alpha_1^{***} &= \alpha_1^{**} - \lambda_1\lambda_2\left[\frac{(Q_{11}+Q_{12})(b_1+b_2)c_1}{(s_{11}+s_{12})(1+b_1+b_2)}+\frac{(Q_{11}-Q_{12})(b_4+b_5)c_2}{(s_{11}-s_{12})(1+b_4+b_5)}\right]\\
&+(1-\lambda_1)\lambda_2\left[\frac{(Q_{11}+Q_{12})c_1}{(s_{11}^p+s_{11}^p)}\left(\frac{1}{b_1}+\frac{1}{1+b_1+b_2}\right)+\frac{(Q_{11}-Q_{12})c_2}{(s_{11}^p-s_{11}^p)}\left(\frac{1}{b_4}-\frac{1}{1+b_4+b_5}\right)\right]\\
&+(1-\lambda_2)\left[\frac{(Q_{11}+Q_{12})c_1}{(s_{11}^s+s_{11}^s)(1+b_1+b_2)}-\frac{(Q_{11}-Q_{12})c_2}{(s_{11}^p-s_{11}^p)(1+b_4+b_5)}\right],\\
\alpha_2^{***} &= \alpha_1^{**} - \lambda_1\lambda_2\left[\frac{(Q_{11}+Q_{12})(b_1+b_2)c_1}{(s_{11}+s_{12})(1+b_1+b_2)}-\frac{(Q_{11}-Q_{12})(b_4+b_5)c_2}{(s_{11}-s_{12})(1+b_4+b_5)}\right]\\
&+(1-\lambda_1)\lambda_2\left[\frac{(Q_{11}+Q_{12})c_1}{(s_{11}^p+s_{11}^p)}\left(\frac{1}{b_1}+\frac{1}{1+b_1+b_2}\right)-\frac{(Q_{11}-Q_{12})c_2}{(s_{11}^p-s_{11}^p)}\left(\frac{1}{b_4}-\frac{1}{1+b_4+b_5}\right)\right]\\
&+(1-\lambda_2)\left[\frac{(Q_{11}+Q_{12})c_1}{(s_{11}^s+s_{11}^s)(1+b_1+b_2)}+\frac{(Q_{11}-Q_{12})c_2}{(s_{11}^p-s_{11}^p)(1+b_4+b_5)}\right],\\
\alpha_3^{***} &= \alpha_3^{**} - \lambda_1\lambda_2\frac{2Q_{12}(b_1+b_2)c_1}{(s_{11}+s_{12})(1+b_1+b_2)}+(1-\lambda_1)\lambda_2\frac{2Q_{12}c_1}{(s_{11}^p+s_{11}^p)}\left(\frac{1}{b_1}+\frac{1}{1+b_1+b_2}\right)\\
&+(1-\lambda_2)\frac{2Q_{12}c_1}{(s_{11}^s+s_{11}^s)(1+b_1+b_2)},\\
\alpha_6^{***} &= -\left[\frac{\lambda_1\lambda_2}{s_{44}}+\frac{(1-\lambda_1)\lambda_2}{s_{44}^p}+\frac{(1-\lambda_2)}{s_{44}^s}\right]\frac{Q_{44}(1-\lambda_1)B_2s_{44}M_1M_2}{b_3^2\lambda_1M_s^2}\\
&+\frac{2B_2Q_{44}(1-\lambda_1)\lambda_2M_1M_2}{b_3M_s^2},
\end{aligned}
\tag{A2}
$$

$$\begin{aligned}\langle F_M^* \rangle = {} & \lambda_1\lambda_2\left\{\frac{1}{s_{11}+s_{12}}\left(c_1^2+2c_0c_1\right)+\frac{1}{s_{11}-s_{12}}c_2^2+\frac{(1-\lambda_1)^2B_2^2s_{44}}{2b_3^2\lambda_1^2M_s^4}M_1^2M_2^2\right\}\\ & +(1-\lambda_1)\lambda_2\left\{-\mathbf{M}\times\mathbf{H}_i+\frac{K_1}{M_s^4}\left(M_1^2M_2^2+M_2^2M_3^2+M_1^2M_3^2\right)+\frac{1}{s_{11}^p+s_{12}^p}\left[c_1^2+2\left(c_0-u_m^p\right)c_1\right]+\frac{1}{s_{11}^p-s_{12}^p}c_2^2\right.\\ & +\frac{2(1+b_1+b_2)}{\left(s_{11}^p+s_{12}^p\right)b_1}c_1\left(c_0-u_m^p+c_1\right)+\frac{B_1}{M_s^2}\left(M_1^2-M_2^2\right)c_2-\frac{\left(s_{11}^p+2s_{12}^p\right)\left(s_{11}^p-s_{12}^p\right)B_1}{2\left(s_{11}^p+s_{12}^p\right)M_s^4}M_3^4\\ & \left.-\left[\frac{(1-\lambda_1)B_2^2s_{44}}{b_3\lambda_1M_s^4}-\frac{(1-\lambda_1)^2B_2^2s_{44}^2}{2s_{44}^pb_3^2\lambda_1^2M_s^4}\right]M_1^2M_2^2-\frac{s_{44}^pB_2^2}{2M_s^4}\left(M_2^2M_3^2+M_1^2M_3^2\right)\right\}\\ & +(1-\lambda_2)\left\{\frac{1}{s_{11}^s+s_{12}^s}\left[c_1^2+2\left(c_0-u_m^p-u_m^s\right)c_1\right]+\frac{1}{s_{11}^s-s_{12}^s}c_2^2+\frac{(1-\lambda_1)^2B_2^2s_{44}^2}{2s_{44}^sb_3^2\lambda_1^2M_s^4}M_1^2M_2^2\right\},\end{aligned}\tag{A3}$$

and

$$c_0=\frac{1}{1+b_1+b_2}\left[(b_1+b_2)u_m^p+b_2u_m^s\right],\tag{A4}$$

$$\begin{aligned}c_1 &= \frac{b_1B_1}{2(1+b_1+b_2)M_s^2}\left[2s_{12}^pM_3^2+\left(s_{11}^p+s_{12}^p\right)\left(M_1^2+M_2^2\right)\right],\\ c_2 &= \frac{b_4B_1}{2(1+b_4+b_5)M_s^2}\left(s_{11}^p-s_{12}^p\right)\left(M_1^2-M_2^2\right).\end{aligned}\tag{A5}$$

Particularly, for $\mathbf{M}=M_s(0,0,1)$, Eqs. (A2) and (A5) become

$$\begin{aligned}\alpha_1^{***} &= \alpha_1^{**}+(Q_{11}+Q_{12})c_1\left[-\frac{\lambda_1\lambda_2(b_1+b_2)}{(s_{11}+s_{12})(1+b_1+b_2)}+\frac{(1-\lambda_1)\lambda_2}{\left(s_{11}^p+s_{11}^p\right)}\left(\frac{1}{b_1}+\frac{1}{1+b_1+b_2}\right)+\frac{(1-\lambda_2)}{\left(s_{11}^s+s_{11}^s\right)(1+b_1+b_2)}\right],\\ \alpha_2^{***} &= \alpha_1^{***},\\ \alpha_3^{***} &= \alpha_3^{**}+2Q_{12}c_1\left[-\frac{\lambda_1\lambda_2(b_1+b_2)}{(s_{11}+s_{12})(1+b_1+b_2)}+\frac{(1-\lambda_1)\lambda_2}{\left(s_{11}^p+s_{11}^p\right)}\left(\frac{1}{b_1}+\frac{1}{1+b_1+b_2}\right)+\frac{(1-\lambda_2)}{\left(s_{11}^s+s_{11}^s\right)(1+b_1+b_2)}\right],\\ \alpha_6^{***} &= 0.\end{aligned}\tag{A6}$$

and

$$\begin{aligned}c_1 &= \frac{b_1B_1s_{12}^p}{1+b_1+b_2},\\ c_2 &= 0.\end{aligned}\tag{A7}$$

References

Bichurin, M. I., Petrov, V. M., Ryabkov, O. V., Averkin, S. V., & Srinivasan, G. (2005). *Physical Review B, 72*, 060408.
Bruno, P., & Chappert, C. (1991). *Physical Review Letter, 67*, 1602–1605.
Diéguez, O., Tinte, S., Antons, A., Bungaro, C., Neaton, J. B., Rabe, K. M., et al (2004). *Physical Review B, 69*, 212101.
Eerenstein, W., Mathur, N. D., & Scott, J. F. (2006). *Nature (London), 442*, 759–765.
Eerenstein, W., Wiora, M., Prieto, J. L., Scott, J. F., & Mathur, N. D. (2007). *Nature Materials, 6*, 348–351.
Fiebig, M. (2005). *Journal of Physics D: Applied Physics, 38*, R123–R152.
Gao, H., & Nix, W. D. (1999). *Annual Review of Materials Science, 29*, 173–209.
Grünberg, P. (2000). *Acta Materialia, 48*, 239–251.
Hill, N. A. (2000). *The Journal of Physical Chemistry B, 104*, 6694–6709.
Ikeda, S., Hayakawa, J., Lee, Y. M., Matsukura, F., Ohno, Y., Hanyu, T., et al (2007). *IEEE Transactions on Electron Devices, 54*, 991–1002.
Junquera, J., & Ghosez, P. h. (2003). *Nature (London), 422*, 506–509.
Li, Y. L., Cross, L. E., & Chen, L. Q. (2005). *Journal Applied Physics, 98*, 064101.
Liu, G., Nan, C. W., Xu, Z. K., & Chen, H. (2005). *Journal of Physics D, 38*, 2321–2326.
Luo, X., Wang, B., & Zheng, Y. (2011). *ACS Nano, 5*(3), 1649–1656.
Murugavel, P., Padhan, P., & Prellier, W. (2004). *Applied Physics Letters, 85*, 4992.
Nan, C. W., Bichurin, M. I., Dong, S. X., Viehland, D., & Srinivasan, G. (2008). *Journal Applied Physics, 103*, 031101.
Newnham, R. E., Skinner, D. P., & Cross, L. E. (1978). *Materials Research Bulletin, 13*, 525–536.
Nix, W. D. (1989). *Metallurgical and Materials Transactions A, 20*, 2217–2245.
O'Handley, R. C., Murray, S. J., Marioni, M., Nembach, H., & Allen, S. M. (2000). *Journal Applied Physics, 87*, 4712–4717.
Pertsev, N. A. (2008). *Physical Review B, 78*, 212102.
Pertsev, N. A., & Kohlstedt, H. (2010). *Nanotechnology, 21*, 475202.
Pertsev, N. A., Kohlstedt, H., & Dkhil, B. (2009). *Physical Review B, 80*, 054102.
Pertsev, N. A., Kukhar, V. G., Kohlstedt, H., & Waser, R. (2003). *Physical Review B, 67*, 054107.
Pertsev, N. A., Tagantsev, A. K., & Setter, N. (2000). *Physical Review B, 61*, R825–R829.

Pertsev, N. A., Zembilgotov, A. G., & Tagantsev, A. K. (1998). *Physical Review Letter, 80*, 1988–1991.
Prokhorenko, S., and Pertsev, N.A., 2010. submitted.
Saha, R., & Nix, W. D. (2002). *Acta Materialia, 50*, 23–28.
Sai, N., Kolpak, A. M., & Rappe, A. M. (2005). *Physical Review B, 72*, 020101. R.
Sang, Y. L., Liu, B., & Fang, D. N. (2008). *Computational Materials Science, 44*.
Srinivasan, G., Rasmussen, E. T., & Hayes, R. (2003). *Physical Review B, 67*, 014418.
Suo, Z. G., & Zhang, Z. Y. (1998). *Physical Review B, 58*, 5116–5120.
Tagantsev, A. K., Gerra, G., & Setter, N. (2008). *Physical Review B, 77*, 174111.
Thiele, C., Dörr, K., Bilani, O., Rödel, J., & Schultz, L. (2007). *Physical Review B, 75*, 054408.
Wang, B., & Woo, C. H. (2005). *Journal Applied Physics, 97*, 084109.
Wang, J., Zhang, Y., Ma, J., Lin, Y., & Nan, C. W. (2008). *Journal Applied Physics, 104*, 014101.
Wu, T., Zurbuchen, M. A., Saha, S., Wang, R-V., Streiffer, S. K., & Mitchell, J. F. (2006). *Physical Review B, 73*, 134416.
Zembilgotov, A. G., Pertsev, N. A., Böttger, U., & Waser, R. (2005). *Applied Physics Letters, 86*, 052903.
Zheng, Y., Wang, B., & Woo, C. H. (2006a). *Applied Physics Letters, 88*, 092903.
Zheng, Y., Wang, B., & Woo, C. H. (2006b). *Applied Physics Letters, 89*, 083115.
Zheng, Y., Wang, B., & Woo, C. H. (2007). *Journal of the Mechanics and Physics of Solids, 55*, 1661–1676.
Zhong, W. L., Wang, Y. G., Zhang, P. L., & Qu, B. D. (1994). *Physical Review B, 50*, 698–703.